Applied Catalysis B: Environment and Energy 350 (2024) 123916

Contents lists available at ScienceDirect

Applied Catalysis B: Environment and Energy

journal homepage: www.elsevier.com/locate/apcatb

Photoelectron migration monitored by 3d orbital electron configuration of spinel cocatalysts for covalent organic framework-based photocatalytic hydrogen evolution

Wenhao He [a], Ke Kong [a,b], Meiying Wang [a], Beibei Dong [a,*], Daqiang Yuan [b], Konstantin P. Bryliakov [c], Ruihu Wang [a,b,**]

[a] Hebei Key Laboratory of Functional Polymer, School of Chemical Engineering and Technology, Hebei University of Technology, Tianjin 300130, China
[b] State Key Laboratory of Structural Chemistry, Fujian Institute of Research on the Structure of Matter, Chinese Academy of Sciences Fuzhou, Fujian 350002, China
[c] Zelinsky Institute of Organic Chemistry RAS, Leninsky prospekt 47, Moscow 119991, Russia

ARTICLE INFO

Keywords:
Covalent organic frameworks
Photocatalysis hydrogen production
3d orbital electron configuration
Cocatalyst
Spinel

ABSTRACT

Covalent organic frameworks (COFs) are promising polymer semiconductors in solar-driven hydrogen production. It is pivotal to promote separation and transfer of charge carriers for achieving high hydrogen evolution efficiency. Herein, we presented one type of noble-metal-free photocatalytic systems by integrating typical ketoenamine-linked TpPa-COF with spinel-structured ACo_2O_4 (ACo_2O_4/TpPa-COF, A = Cu, Ni, Fe). The 3d orbital electron configurations of metal ions in ACo_2O_4 regulate the photogenerated electrons transfer from the conductive band of TpPa-COF to the active sites of cocatalyst. The $3d^9$ orbital configuration and electron-rich capability of $CuCo_2O_4$ have been evidenced to boost the directional migration of charge carriers, thus significantly expediting photocatalytic hydrogen evolution kinetics. The hydrogen evolution rate in $CuCo_2O_4$/TpPa-COF is up to 8346 μmol g^{-1} h^{-1}, which surpasses those in their physical mixture (3769 μmol g^{-1} h^{-1}), and is even higher than that of Pt-loaded TpPa-COF (7587 μmol g^{-1} h^{-1}). This work provides new protocols to construct noble-metal-free COF-based photocatalytic systems for solar-to-chemical conversion.

1. Introduction

Solar-driven photocatalytic hydrogen production is regarded as one promising technology for converting solar energy into green hydrogen [1–6]. Covalent organic frameworks (COFs) are one new type of crystalline polymer semiconductors with porous network topologies, and display many advantages for solar-driven water splitting owing to their long-range order structures, large surface areas, wide visible light absorbance range and tunable band gaps [7–10]. However, majority of COFs are constructed through typical Schiff-base condensation reaction, the resultant organic linkages, such as imine and hydrazone, possess high polarity, the concomitantly discontinuous π-electron delocalization is unfavorable for the migration of the photogenerated charge carriers in the host backbones [11–13]. Moreover, most of as-prepared COFs are lack of metal centers, metal-containing cocatalysts are usually required to achieve high photocatalytic efficiencies [14–16]. The cocatalyst itself is inactive or has little photocatalytic activity, but they could provide catalytic active sites for the conversion of the proton to hydrogen. The directional migration of the photogenerated electrons from COFs to the active sites of the cocatalysts induces the photocatalytic reaction [17]. However, hydrogen production rate in majority of COFs-based photocatalytic systems is lower than that of Pt-based counterparts owing to inefficient separation of the photogenerated electron-hole pairs and relatively high over-potential of proton reduction. It is of great significance to tailor-make noble-metal-free cocatalysts as Pt-alternatives for hydrogen evolution reaction.

An effective strategy is to construct COFs-based semiconductor dyads with strong interfacial effects that make sure smoothly opposite migration of the photogenerated electrons and holes [18,19]. It is well documented that the nanostructured spinel materials are promising alternatives to noble metal catalysts due to their low cost, environment-benign nature, high earth abundance and strong resistance

* Corresponding author.
** Corresponding author at: Hebei Key Laboratory of Functional Polymer, School of Chemical Engineering and Technology, Hebei University of Technology, Tianjin 300130, China.
E-mail addresses: bbdong@hebut.edu.cn (B. Dong), ruihu@fjirsm.ac.cn (R. Wang).

https://doi.org/10.1016/j.apcatb.2024.123916
Received 15 January 2024; Received in revised form 29 February 2024; Accepted 3 March 2024
Available online 7 March 2024

to poisoning [20–24]. ACo_2O_4 (A = Cu, Ni, Fe et. al), as one type of stable metal oxides, possesses superior conductivity and electrochemical properties when compared with single divalent metal oxides or Co_3O_4 [25]. A large number of partially filled 3d orbitals in A^{2+} and Co^{3+} ($3d^6$) allow ACo_2O_4 to work as an electron collector, the photogenerated electrons could be partly transferred from the photocatalysts to the active sites of ACo_2O_4, resulting in directional charge separation and the decrease of electron/hole recombination [26–29]. Moreover, good compatibility between COFs and spinel-structured materials allows their interfacial space to induce a built-in electric field, thus decreasing charge transfer activation energy [30,31]. The composition of COFs and ACo_2O_4 could integrate their advantages in terms of incident light absorption efficiency, the migration of the photoinduced carriers and the available catalytic active sites, thus cooperatively inducing high photocatalytic activity in hydrogen evolution reaction. However, the effects of the electronic configurations in divalent metals of the spinels on the photocatalytic activity remains unclear. An in-depth fundamental understanding of relationships between divalent metals and photocatalytic activity is indispensable to rationally construct noble-metal-free photocatalysts for task-specific application.

As a proof-of-concept study, herein, we reported one type of noble-metal-free photocatalytic systems by combining ketoenamine-linked TpPa-COF with spinel-structured ACo_2O_4 (ACo_2O_4/TpPa-COF, A = Cu, Ni, Fe). The diversity of divalent metals in ACo_2O_4 provides great opportunities to understand the effects of their electronic configurations on photocatalytic activity. To the best of our knowledge, this is the first report for COFs-based photocatalytic systems with spinel cocatalysts. Although either TpPa-COF or $CuCo_2O_4$ shows negligible photocatalytic activity under visible light irradiation, hydrogen evolution rate in $CuCo_2O_4$/TpPa-COF exceeds those in Pt-based counterpart and majority of COFs-based photocatalytic systems. The promising photocatalytic activity is essentially attributed to the decrement of water reduction over-potentials and the promotion of the photogenerated electrons transfer from the conduction band of TpPa-COF to the active sites of $CuCo_2O_4$. This work provides one type of noble-metal-free cocatalysts for COF-based photocatalytic hydrogen evolution reaction.

2. Experimental section

2.1. Preparation of ACo_2O_4

$CuCo_2O_4$ spinel was prepared according to the modified literature method [32]. $Cu(NO_3)_2{\cdot}3\ H_2O$ (0.483 g, 2.0 mmol), $Co(NO_3)_2{\cdot}6\ H_2O$ (1.164 g, 4.0 mmol) and urea (1.08 g, 18 mmol) in deionized water (60 mL) were stirred at room temperature for 20 min. The solution was transferred to a Teflon-lined stainless-steel autoclave, and the reactor was sealed and heated at 120 °C for 6 h. After cooling to room temperature, the resultant solid was filtered, washed several times with water/ethanol, and dried overnight at 80 ℃, subsequent calcination in the air stream at 300 ℃ for 3 h gave rise to $CuCo_2O_4$.

$NiCo_2O_4$ and $FeCo_2O_4$ were prepared using the same procedures except $Cu(NO_3)_2{\cdot}3\ H_2O$ were replaced by $Ni(NO_3)_2{\cdot}6\ H_2O$ and $Fe(NO_3)_3{\cdot}9\ H_2O$, respectively.

2.2. Preparation of TpPa-COF

TpPa-COF was prepared according to the modified literature method [18]. Triformylphloroglucinol (63 mg, 0.3 mmol), 2,5-dimethyl-p-phenylenediamine (61.3 mg, 0.45 mmol), mesitylene (1.5 mL), dioxane (1.5 mL) and aqueous acetic acid solution (0.5 mL, 3 M) were added into a 10 mL Pyrex tube. The Pyrex tube containing the reaction mixture was ultrasonicated for 10 min, and then degassed three times in liquid nitrogen through freezing-pump-thawing cycle. After heated at 120 ℃ for 3 days and cooling to room temperature, red precipitate was collected by filtration and washed several times with tetrahydrofuran, subsequent treatment under vacuum at 60 ℃ overnight gave rise to TpPa-COF.

2.3. Preparation of ACo_2O_4/TpPa-COF

The synthetic procedures are similar to that of TpPa-COF except the extra addition of suitable amount of ACo_2O_4 in the starting materials. Unless otherwise noted, ACo_2O_4/TpPa-COF refers specifically to a mass content of ACo_2O_4 to TpPa-COF of 5 wt%.

3. Results and discussion

3.1. Materials synthesis and characterizations

Taking $CuCo_2O_4$/TpPa-COF as an example, the synthetic route is depicted in Fig. 1**a.** $CuCo_2O_4$ spinel was synthesized by hydrothermal reaction of copper nitrate, cobalt nitrate and urea at 120 °C, followed by the calcination treatment in air at 300 °C. The condensation reaction of triformylphloroglucinol (TP) and 2,5-dimethyl-p-phenylenediamine (DMPA) in the presence of as-prepared $CuCo_2O_4$ in mesitylene/dioxane/acetic acid gave rise to $CuCo_2O_4$/TpPa-COF.

Scanning electron microscopy (SEM) image exhibits that TpPa-COF is composed of nanosheets (Fig. 1**b**), while $CuCo_2O_4$ shows nanoflower morphology consisting of the aggregated needle-shaped structure (Fig. S1). The nanosheets morphology is maintained in $CuCo_2O_4$/TpPa-COF, but they are rougher and thicker than that of TpPa-COF (Fig. 1**c**). $CuCo_2O_4$ and TpPa-COF are intimately attached with each other, which is further confirmed by transmission electron microscope (TEM) images (Fig. S2). The lattice distance of 0.245 nm in high-resolution TEM (HRTEM) image of $CuCo_2O_4$/TpPa-COF accounts for (311) lattice fringe of $CuCo_2O_4$ spinel (Fig. 1**d**). The intimate contact between TpPa-COF and $CuCo_2O_4$ could be clearly identified. The high-angle annular dark-field scanning TEM (HAADF-STEM) and elemental mapping images corroborate homogeneous distribution of C, N, O, Co and Cu elements in $CuCo_2O_4$/TpPa-COF (Fig. 1**e,** S3).

The structures of TpPa-COF and $CuCo_2O_4$/TpPa-COF were confirmed by powder X-ray diffraction (XRD) and Fourier transform infrared (FT-IR) spectra. In XRD pattern of TpPa-COF, the characteristic diffraction peaks at 4.6 and 26.7° correspond to the (100) and (001) facets, respectively (Fig. 2**a**), which reveals that TpPa-COF crystallizes in the monoclinic P2 space group [33]. The diffraction peaks of $CuCo_2O_4$ match well with the peaks of standard AB_2O_4 spinel (Fig. S4) [32,34]. The XRD pattern of $CuCo_2O_4$/TpPa-COF is the same as that of TpPa-COF, and the absence of typical peaks for $CuCo_2O_4$ is attributed to weak crystallinity of $CuCo_2O_4$ and low content of 5% $CuCo_2O_4$ in the dyad. When weight percentage of $CuCo_2O_4$ in the starting materials is increased from 5% in $CuCo_2O_4$/TpPa-COF to 10% and 20%, one new peak occurs at 37°, which is assigned to the (311) crystal plane of $CuCo_2O_4$. Moreover, the integration of $CuCo_2O_4$ with TpPa-COF has negligible effects on the structure of TpPa-COF (Fig. S4), which is evidenced by the identical FT-IR spectra of TpPa-COF and $CuCo_2O_4$/TpPa-COF (Fig. 2**b, S5**). The stretching vibration peaks at 1578 and 1255 cm^{-1} correspond to C═C and C-N, respectively, validating the formation of β-ketoenamine-linked skeleton [35].

The permanent porosities were examined by nitrogen adsorption-desorption measurements at 77 K (Fig. 2**c**). TpPa-COF and $CuCo_2O_4$/TpPa-COF exhibit typical type I isotherm, indicative of their microporous structures. The pore size distributions show that their pores are centered at 12.5 Å (Fig. S6). The Brunauer-Emmett-Teller (BET) specific surface areas of $CuCo_2O_4$, TpPa-COF and $CuCo_2O_4$/TpPa-COF are 94.68, 611.92 and 483.94 $m^2\ g^{-1}$, respectively. The slight decrease of BET specific surface area of $CuCo_2O_4$/TpPa-COF compared with TpPa-COF is attributed to the introduction of $CuCo_2O_4$. Thermogravimetric analysis (TGA) curves show that TpPa-COF and $CuCo_2O_4$/TpPa-COF are stable before 350 °C under N_2 atmosphere (Fig. 2**d**), and the combination of $CuCo_2O_4$ with TpPa-COF has negligible effects on thermal stability of TpPa-COF.

X-ray photoelectron spectroscopy (XPS) survey spectrum of $CuCo_2O_4$/TpPa-COF indicates the presence of C, N, O, Cu and Co

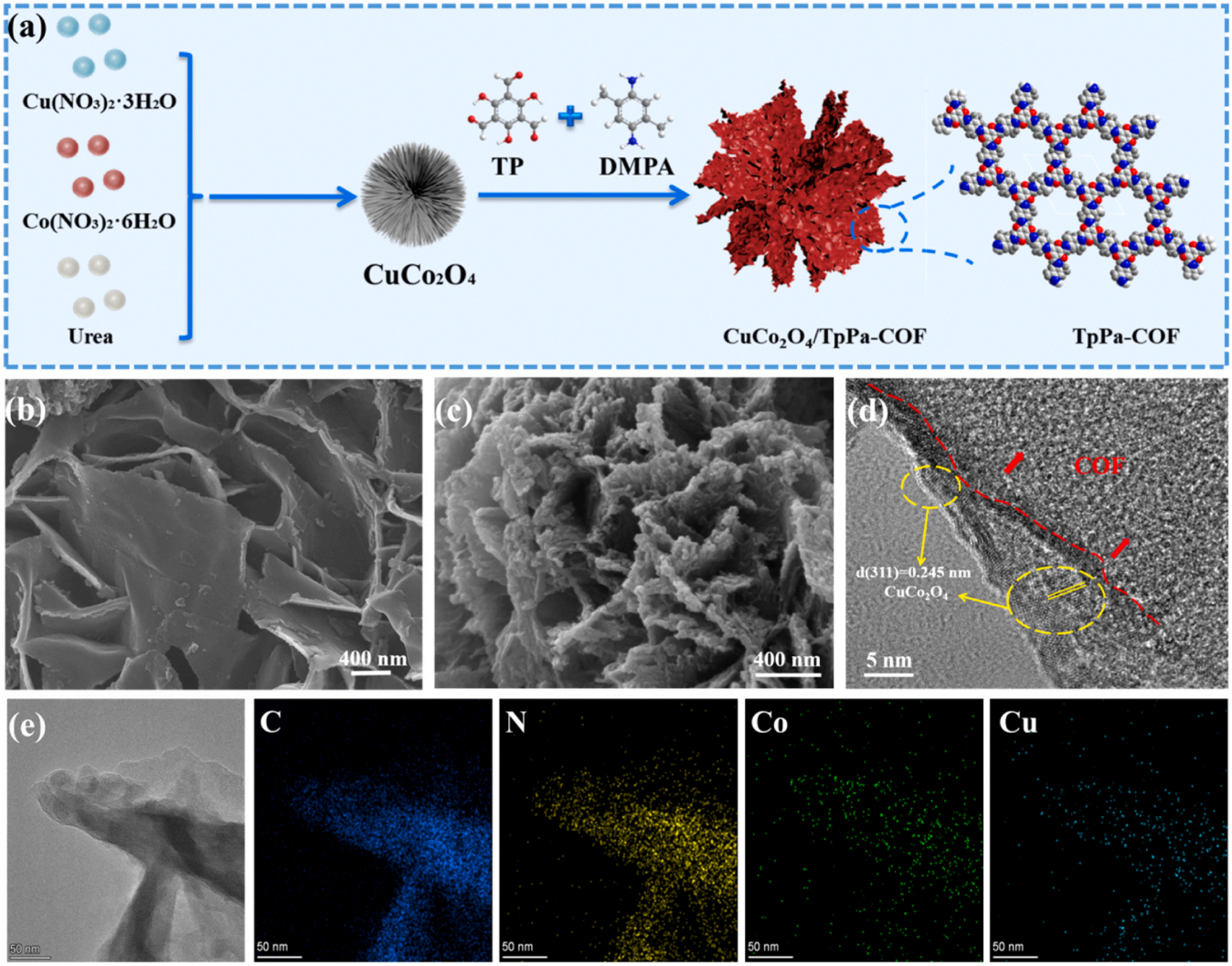

Fig. 1. (a) Schematic diagram for the preparation of $CuCo_2O_4$/TpPa-COF. SEM images for (b) TpPa-COF and (c) $CuCo_2O_4$/TpPa-COF. (d) HRTEM and (e) EDS element mapping images of $CuCo_2O_4$/TpPa-COF.

elements (Fig. 2**e**), which suggests the combination of $CuCo_2O_4$ and TpPa-COF in $CuCo_2O_4$/TpPa-COF. In the high-resolution C 1 s XPS spectrum of TpPa-COF, the binding energy peaks at 284.6, 285.7 and 288.4 eV are assigned to C-C/C═C, C-N and C═O bonds, respectively (Fig. 2**f**), which further confirms the *β*-ketoenamine structure of TpPa-COF [36]. The deconvoluted N 1 s XPS spectrum provides one peak at 399.7 eV (Fig. 2**g**), corresponding to C-N bond of TpPa-COF. A positive shift by 0.2 eV is observed in $CuCo_2O_4$/TpPa-COF owing to the electron donation of nitrogen atom to Cu and Co. The high-resolution Cu 2p spectrum of $CuCo_2O_4$ could be fitted into four peaks (Fig. 2**h**). The peaks at 934.1 and 954 eV are assigned to Cu $2p_{3/2}$ and Cu $2p_{1/2}$, respectively, while the peaks at 941.8 and 962.3 eV are the satellite peaks (marked as "Sat."). In the high-resolution Co 2p XPS spectrum of $CuCo_2O_4$ (Fig. 2**i**), two binding energy peaks at 780.8 and 795.9 eV belong to Co $2p_{3/2}$ and Co $2p_{1/2}$ spin orbit peaks, respectively, and other peaks at 789 eV and 804.9 eV are the satellite peaks [37]. The binding energy peaks of Cu 2p and Co 2p in $CuCo_2O_4$/TpPa-COF are negatively shifted by *ca.* 0.5 eV and 0.2 eV when compared with those of $CuCo_2O_4$, respectively. The peak shift not only indicates close interaction between the solid-solid interface of $CuCo_2O_4$ and TpPa-COF, but also validates the electron transfer from TpPa-COF to $CuCo_2O_4$, which could promote the directional separation and transfer of charge carriers in photocatalytic reaction [30,38].

3.2. Photocatalytic hydrogen evolution performance

In UV–vis diffuse reflectance spectra (UV–vis DRS), TpPa-COF and $CuCo_2O_4$/TpPa-COF exhibit strong visible light response with similar light absorption edge of *ca.* 630 nm, while $CuCo_2O_4$ shows full absorption in the range from 200 to 800 nm (Fig. 3**a**). The band gap energy values of TpPa-COF and $CuCo_2O_4$/TpPa-COF are calculated by Tauc equation to be 2.04 and 2.02 eV, respectively (Fig. 3**b**). Mott-Schottky curves show that the flat-band potentials (E_{fb}) of TpPa-COF and $CuCo_2O_4$/TpPa-COF are *ca.* −0.68 and −0.55 V *vs.* normal hydrogen electrode (NHE), respectively (Fig. 3**c,** S7). The positive slopes of the tangent lines in the Mott-Schottky curves reveal n-type characteristics of TpPa-COF and $CuCo_2O_4$/TpPa-COF [39]. The conduction band (CB) positions of n-type semiconductors are usually more negative (-0.1 V) than the flat band potentials [35,40]. Thus, the CB potentials of TpPa-COF and $CuCo_2O_4$/TpPa-COF are estimated to be *ca.* −0.78 and −0.65 V *vs.* NHE, respectively. The valence band (VB) potentials of TpPa-COF and $CuCo_2O_4$/TpPa-COF are calculated to be 1.26 and 1.37 V, respectively. Therefore, both TpPa-COF and $CuCo_2O_4$/TpPa-COF possess suitable energy band structures to meet the conditions for hydrogen production from photocatalytic water splitting.

Photocatalytic hydrogen evolution performance of TpPa-COF and $CuCo_2O_4$/TpPa-COF was evaluated under visible light irradiation using L-ascorbic acid as a sacrificial reagent in the absence of noble metal. As

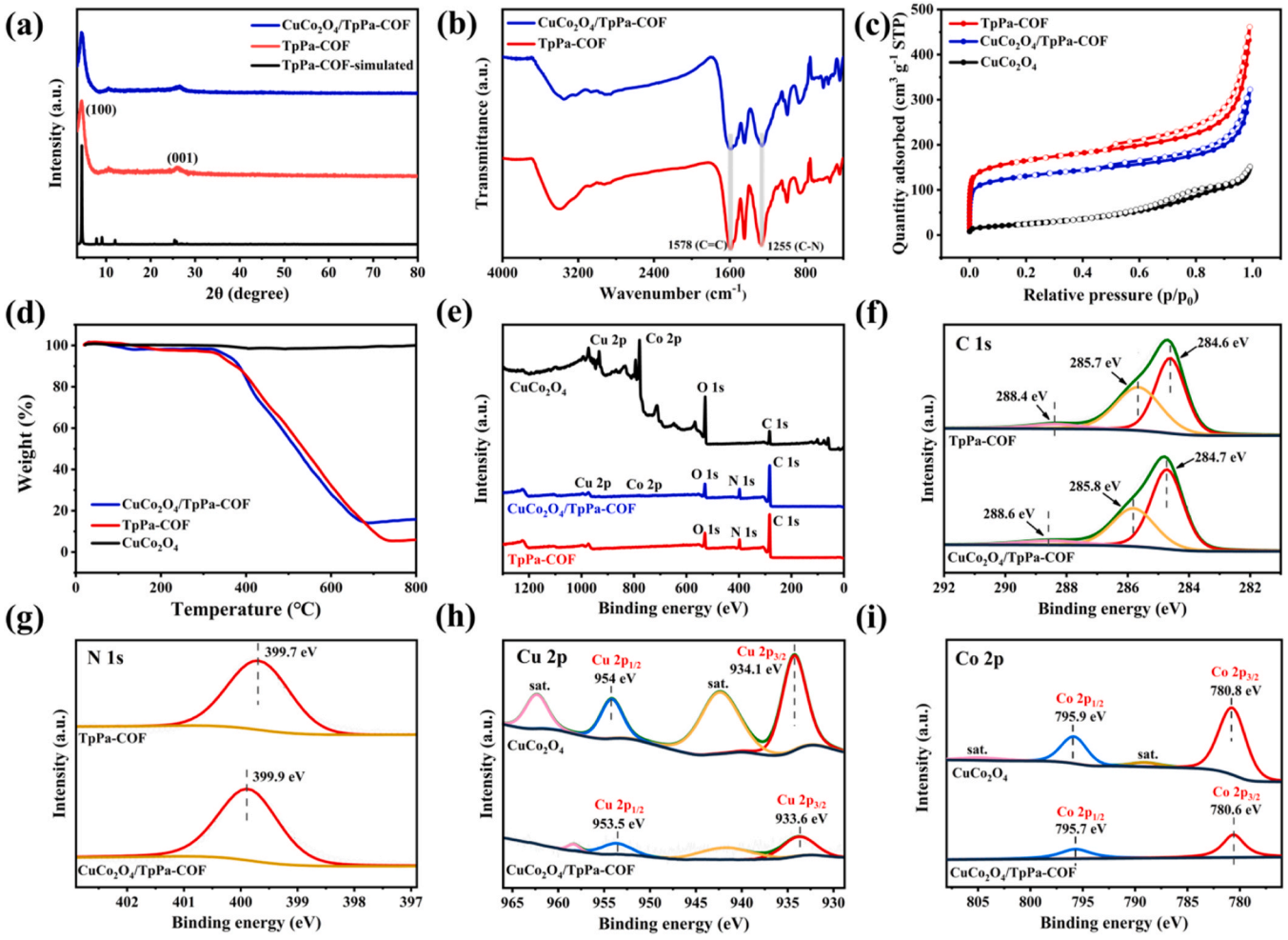

Fig. 2. (a) XRD patterns and (b) FT-IR spectra of TpPa-COF and $CuCo_2O_4$/TpPa-COF. (c) N_2 sorption isotherms and (d) TGA curves for TpPa-COF, $CuCo_2O_4$ and $CuCo_2O_4$/TpPa-COF. (e) The XPS survey spectra of $CuCo_2O_4$, $CuCo_2O_4$/TpPa-COF and TpPa-COF. High-resolution XPS spectra of (f) C 1 s and (g) N 1 s for TpPa-COF and $CuCo_2O_4$/TpPa-COF. High-resolution XPS spectra of (h) Cu 2p and (i) Co 2p for $CuCo_2O_4$ and $CuCo_2O_4$/TpPa-COF.

shown in Fig. S8 and S9, the loading amount of $CuCo_2O_4$ is closely related to the photocatalytic activity. $CuCo_2O_4$/TpPa-COF with 5% loading amount of $CuCo_2O_4$ provides the highest hydrogen evolution rate as high as 8346 μmol g^{-1} h^{-1} (Fig. S9), which is superior to those in majority of the reported COFs-based photocatalytic systems (Fig. 3**d**, Table S1). The absence of either $CuCo_2O_4$ or TpPa-COF results in poor photocatalytic activity, validating that TpPa-COF serves as a photosensitizer and $CuCo_2O_4$ provides catalytic active sites for hydrogen generation. Small amount of 2.5% $CuCo_2O_4$ in 2.5% $CuCo_2O_4$/TpPa-COF could not provide enough photocatalytic active sites, affording hydrogen evolution rate of 3940 μmol g^{-1} h^{-1}. The excessive amounts of 10% and 20% $CuCo_2O_4$ probably inhibit light absorption process, leading to the declined hydrogen evolution rates of 3336 and 2554 μmol g^{-1} h^{-1}, respectively. Notably, hydrogen evolution rate for physical mixture of $CuCo_2O_4$ and TpPa-COF is 3769 μmol g^{-1} h^{-1}, which is about half of that of $CuCo_2O_4$/TpPa-COF (Fig. 3**e**), revealing that the interfacial interactions between $CuCo_2O_4$ and TpPa-COF could promote photocatalytic activity of the dyad. Meanwhile, the activity of the dyad is also higher than that of 5% Pt/TpPa-COF (7587 μmol g^{-1} h^{-1}), indicating that $CuCo_2O_4$ could serve as promising alternatives of platinum cocatalysts to effectively enhance photocatalytic hydrogen evolution activity of COFs semiconductors. The light-wavelength dependency examination shows that $CuCo_2O_4$/TpPa-COF could utilize a broad range of visible light, and hydrogen production rates under monochromatic light of 420, 450, 500 and 600 nm are 751, 716, 708 and 382 μmol g^{-1} h^{-1}, respectively (Fig. 3**f**). The apparent quantum efficiencies (AQE) are calculated to be 0.78%, 0.71%, 0.69% and 0.38%, respectively. $CuCo_2O_4$/TpPa-COF shows excellent durability and photochemical stability, when the dyad was used for consecutive five times for 25 h in photocatalytic hydrogen evolution reaction, there are no detectable activity loss and structural variation (Fig. 3**g**), the XRD pattern and FT-IR spectrum of post-$CuCo_2O_4$/TpPa-COF are identical with that of as-prepared sample (Fig. S10, S11).

To better clarify the roles of $CuCo_2O_4$ in photocatalytic hydrogen evolution reaction, other ACo_2O_4 (A = Ni, Fe) spinel cocatalysts were also integrated with TpPa-COF to form ACo_2O_4/TpPa-COF dyads. The XRD patterns of $NiCo_2O_4$ and $FeCo_2O_4$ show typical peaks that match well with the peaks of standard AB_2O_4 spinels (Fig. S12) [32,34]. The successful synthesis of ACo_2O_4/TpPa-COF by combining ACo_2O_4 with TpPa-COF was confirmed by their XRD pattern and FI-IR spectra (Fig. S13). UV–vis DRS and the band gap energy values of $NiCo_2O_4$/TpPa-COF and $FeCo_2O_4$/TpPa-COF are very close to those in TpPa-COF and $CuCo_2O_4$/TpPa-COF (Fig. S14a, S14b), suggesting light absorption results from TpPa-COF, and the effects of ACo_2O_4 spinels on light absorption are negligible upon visible light irradiation. Mott-Schottky measurements show CB potentials of $NiCo_2O_4$/TpPa-COF and $FeCo_2O_4$/TpPa-COF are −0.45 and −0.42 V *vs.* NHE, respectively (Fig. S14c, S14d). Obviously, $CuCo_2O_4$/TpPa-COF has more negative CB than $NiCo_2O_4$/TpPa-COF and $FeCo_2O_4$/TpPa-COF, which suggests that $CuCo_2O_4$/TpPa-COF has stronger reducing capacity for hydrogen evolution (Fig. 3**i**). As shown in Fig. 3**h**, the hydrogen evolution rate in $CuCo_2O_4$/TpPa-COF is about 10.3 times and 144 times higher than those

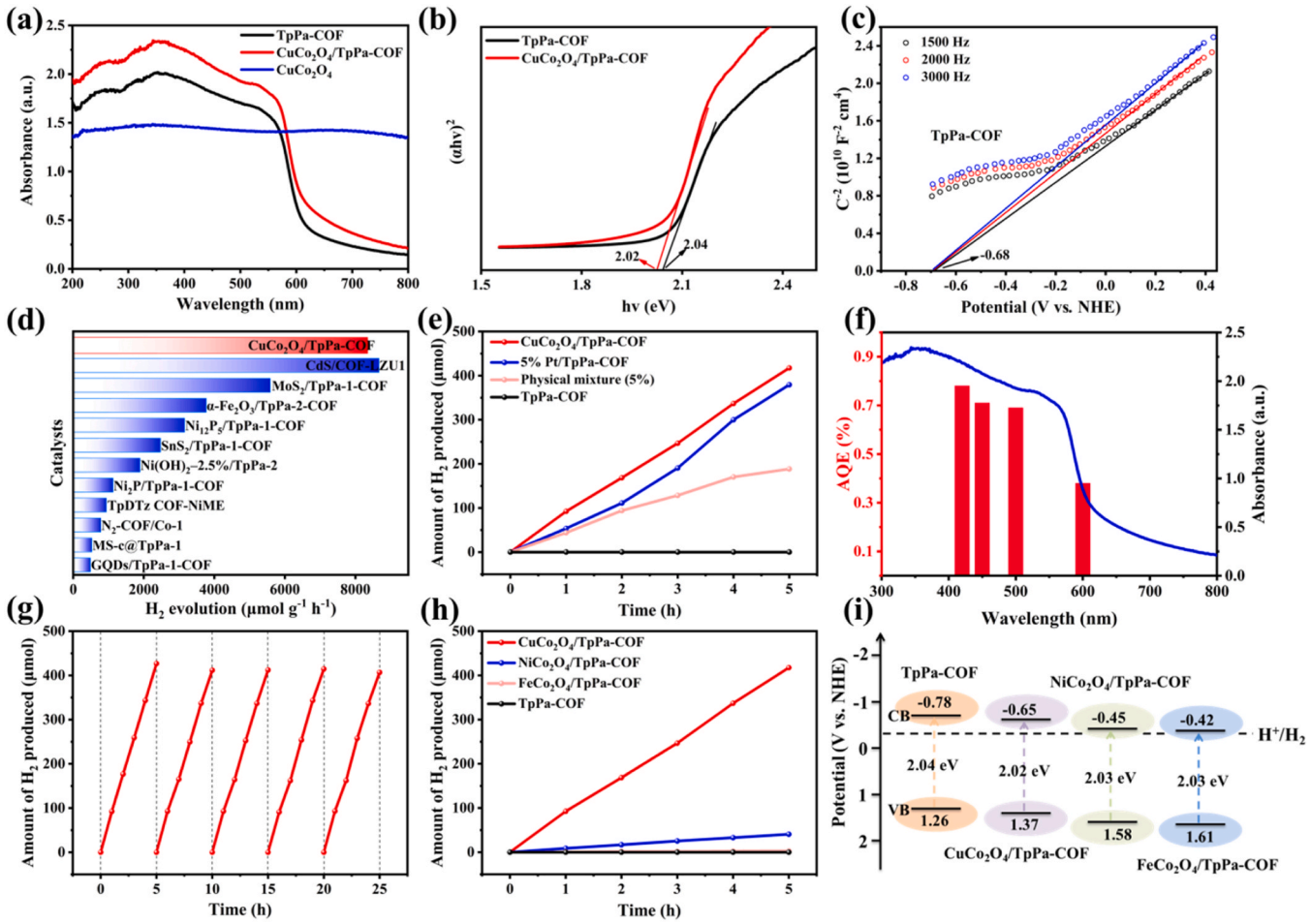

Fig. 3. (a) UV–vis DRS for $CuCo_2O_4$, TpPa-COF and $CuCo_2O_4$/TpPa-COF. (b) Tauc plots for TpPa-COF and $CuCo_2O_4$/TpPa-COF. (c) Mott-Schottky curves of TpPa-COF. (d) The comparison of hydrogen evolution rate of $CuCo_2O_4$/TpPa-COF with the reported noble-metal-free photocatalytic systems. (e) Photocatalytic activities of TpPa-COF, 5% Pt/TpPa-COF, physical mixture of 5% $CuCo_2O_4$ and TpPa-COF, $CuCo_2O_4$/TpPa-COF. (f) The wavelength-dependent hydrogen evolution reaction of $CuCo_2O_4$/TpPa-COF. (g) Hydrogen evolution cycle tests of $CuCo_2O_4$/TpPa-COF. (h) Photocatalytic hydrogen evolution rates of TpPa-COF and ACo_2O_4/TpPa-COF. (i) Energy structure diagrams of TpPa-COF and ACo_2O_4/TpPa-COF. Reaction conditions: unless otherwise stated, photocatalysts (10 mg), L-ascorbic acid (100 mg), H_2O (10 mL), N_2 (1 atm) and visible-light irradiation ($\lambda \geq 420$ nm) for 5 h.

of $NiCo_2O_4$/TpPa-COF (811 μmol g^{-1} h^{-1}) and $FeCo_2O_4$/TpPa-COF (58 μmol g^{-1} h^{-1}), respectively. These results have demonstrated that $CuCo_2O_4$ is a promising noble-metal-free cocatalyst for hydrogen evolution owing to $3d^9$ orbital configuration of Cu^{2+}.

3.3. Mechanism research

The effective generation and instantaneous separation of the photoexcited carriers are the preconditions for photocatalytic reactions. To get insight into the roles of ACo_2O_4 spinel in photocatalytic hydrogen generation, the steady-state photoluminescence (PL) spectra were performed. As shown in Fig. 4**a**, TpPa-COF shows strong and broad emission peaks at 640 nm upon excitation at 380 nm, and the emission peak intensities are in the following trend: TpPa-COF > $FeCo_2O_4$/TpPa-COF > $NiCo_2O_4$/TpPa-COF > $CuCo_2O_4$/TpPa-COF, indicating that the favorable photoelectron transfer from TpPa-COF to $CuCo_2O_4$, the recombination of the photogenerated electron and hole is greatly inhibited in $CuCo_2O_4$/TpPa-COF [41]. The results are further corroborated by time-resolved PL decay spectroscopy, the average lifetime (τ_{avg}) of TpPa-COF, $CuCo_2O_4$/TpPa-COF, $NiCo_2O_4$/TpPa-COF and $FeCo_2O_4$/TpPa-COF are 0.353, 0.465, 0.413 and 0.407 ns, respectively (Fig. 4**b**, Table S2). In the electrochemical impedance spectroscopy (Fig. 4**c**), the semicircular arc radius of TpPa-COF is the largest, the gradual shrunk trend is observed in $FeCo_2O_4$/TpPa-COF, $NiCo_2O_4$/TpPa-COF and $CuCo_2O_4$/TpPa-COF. The smallest arc radius of $CuCo_2O_4$/TpPa-COF shows that $CuCo_2O_4$ greatly reduces the interfacial electron transfer resistance, which is further validated by photocurrent measurements (Fig. 4**d**). The photocurrent density of $CuCo_2O_4$/TpPa-COF is remarkably increased when compared with that of TpPa-COF, $NiCo_2O_4$/TpPa-COF and $FeCo_2O_4$/TpPa-COF [42]. These observations have demonstrated that the integration of ACo_2O_4 and TpPa-COF could promote the separation and migration of charge carriers through their interface, and $CuCo_2O_4$ is the most beneficial for the directional transfer of the photogenerated electron to the active sites owing to its d^9 orbital electron configuration of Cu^{2+}, thus boosting photocatalytic hydrogen evolution reaction.

To better understand photocatalytic hydrogen evolution reaction over $CuCo_2O_4$/TpPa-COF, density functional theory (DFT) calculations were performed. The localized electron distribution on the interface of TpPa-COF and $CuCo_2O_4$ could be clearly detected (Fig. 4**e**). The electron cloud on TpPa-COF is attenuated, while the charge is obviously accumulated on the surface of $CuCo_2O_4$, a built-in electric field in the space charge region between TpPa-COF and $CuCo_2O_4$ is generated, further validating the photoelectron transfer from TpPa-COF to $CuCo_2O_4$, which is well consistent with their high-resolution XPS results and photochemical performance [43].

Based on the aforementioned observations, a plausible mechanism for photocatalytic hydrogen evolution over ACo_2O_4/TpPa-COF has been

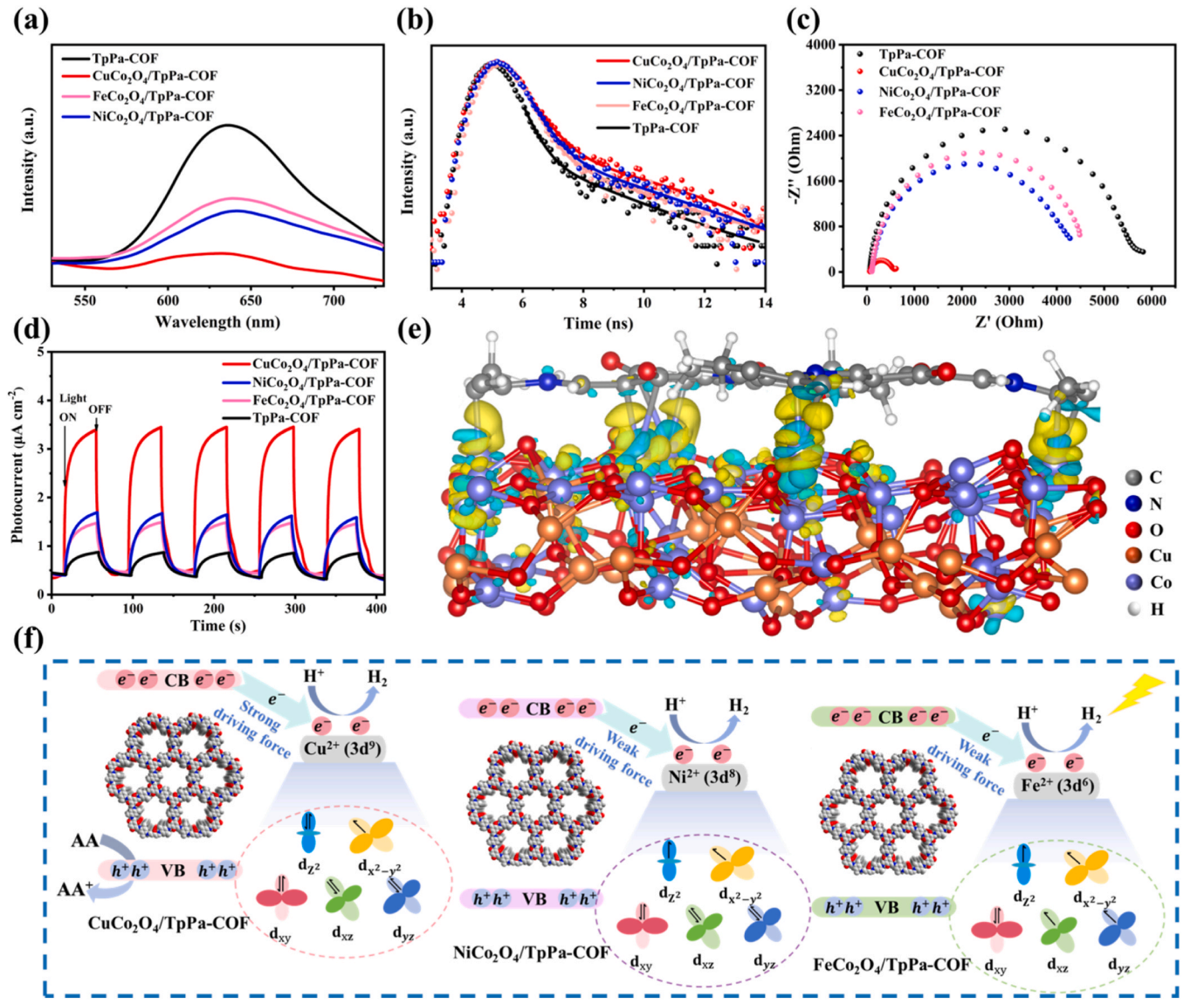

Fig. 4. (a) PL spectra upon the excitation at 380 nm, (b) time-resolved PL spectra, (c) EIS Nyquist plots and (d) transient photocurrent responses of TpPa-COF and ACo_2O_4/TpPa-C0OF. (e) The differential charge density of $CuCo_2O_4$/TpPa-COF with an isovalue of 0.0045e Å^{-3}. The bule and yellow contours represent the charge accumulation and charge depletion, respectively. (f) Illustration of possible photocatalytic hydrogen evolution mechanism over ACo_2O_4/TpPa-COF under visible-light irradiation.

proposed (Fig. 4**f**). TpPa-COF serves as a photosensitizer, the electrons and holes are generated on the surface of TpPa-COF upon visible-light irradiation. $CuCo_2O_4$ serves as an electron collector, strong interfacial interactions between TpPa-COF and $CuCo_2O_4$ could expedite the separation and migration of the photogenerated charge carriers. The photogenerated electrons in the conduction band of TpPa-COF rapidly migrate to the active sites of $CuCo_2O_4$, where the accumulated electrons reduce proton into hydrogen. Meanwhile, the photogenerated holes in the valence band of TpPa-COF are compensated through reacting with L-ascorbic acid (AA) to realize charge balance. Remarkably, TpPa-COF possesses periodic photosensitizer units for sufficient visible light absorption, and $CuCo_2O_4$ provides enough active sites for photocatalytic conversion, in which $3d^9$ orbital electron configuration of Cu^{2+} and electron-enrichment capability of $CuCo_2O_4$ facilitate the transfer of the photogenerated electrons from TpPa-COF to $CuCo_2O_4$, these advantages cooperatively induce high photocatalytic hydrogen evolution efficiency. Although $NiCo_2O_4$ and $FeCo_2O_4$ have similar functions in the photocatalytic reaction, the orbital electron configurations of Ni^{2+} ($3d^8$) and Fe^{2+} ($3d^6$) mitigate the driving force of the photogenerated electron transfer from TpPa-COF to the spinel surface, thus resulting in low photocatalytic activity.

4. Conclusion

One type of noble-metal-free photocatalytic systems based on COFs and ACo_2O_4 spinels have been constructed for visible-light-driven hydrogen evolution reaction. The unique $3d^9$ orbital electron configuration and strong electron-enrichment capability of $CuCo_2O_4$ enable rapid transfer of the photogenerated electrons from TpPa-COF to the active sites of $CuCo_2O_4$ through their interfacial interactions when compared with those of $NiCo_2O_4$ and $FeCo_2O_4$, while rich porosity of TpPa-COF maximally permits the contact of reactant substrate with cocatalysts. The prominent advantages of $CuCo_2O_4$/TpPa-COF remarkedly improve photocatalytic hydrogen evolution kinetics, thus, photocatalytic activity is significantly improved when compared with those in their independent counterparts, physical mixture, and is even higher than that of Pt-based counterpart. This work not only provides new protocols to tailor-make Pt-substituted noble-metal-free cocatalysts for

photocatalytic hydrogen evolution reaction, but also contributes to the development of COFs-based photocatalytic systems for solar-to-chemical conversion.

CRediT authorship contribution statement

Daqiang Yuan: Software. **Ruihu Wang:** Writing – review & editing, Supervision. **Konstantin P. Bryliakov:** Writing – review & editing. **Wenhao He:** Writing – original draft, Conceptualization. **Ke Kong:** Methodology. **Meiying Wang:** Investigation. **Beibei Dong:** Validation, Conceptualization.

Declaration of Competing Interest

The authors declare that they have no known competing financial interests or personal relationships that could have appeared to influence the work reported in this paper.

Data Availability

Data will be made available on request.

Acknowledgements

The authors acknowledge financial supports from the Natural Science Foundation of Hebei Province (B2022202039), S&T Program of Hebei (236Z4308G), National Natural Science Foundation of China (21975259) and National Key Research and Development Program (2019YFA0210403).

Appendix A. Supporting information

Supplementary data associated with this article can be found in the online version at doi:10.1016/j.apcatb.2024.123916.

References

[1] W. Jiang, Y. Zhao, D.X. Zong, H. Nie, L. Niu, L. An, D. Qu, X. Wang, Z. Kang, Z. Sun, Photocatalyst for high-performance H_2 production: Ga-doped polymeric carbon nitride, Angew. Chem. Int. Ed. 60 (2021) 6124.
[2] Y. Wan, L. Wang, H. Xu, X. Wu, J. Yang, A simple molecular design strategy for two-dimensional covalent organic framework capable of visible-light-driven water splitting, J. Am. Chem. Soc. 142 (2020) 4508–4516.
[3] S. Wu, C. Li, Y. Wang, Y. Zhuang, Y. Pan, N. Wen, S. Wang, Z. Zhang, Z. Ding, R. Yuan, W. Dai, X. Fu, J. Long, The keto-switched photocatalysis of reconstructed covalent organic frameworks for efficient hydrogen evolution, Angew. Chem. Int. Ed. 62 (2023) e202309026.
[4] L. Tian, S. Min, F. Wang, Integrating noble-metal-free metallic vanadium carbide cocatalyst with CdS for efficient visible-light-driven photocatalytic H_2 evolution, Appl. Catal. B-Environ. 259 (2019) 118029.
[5] R. Shen, X. Li, C. Qin, P. Zhang, X. Li, Efficient photocatalytic hydrogen evolution by modulating excitonic effects in Ni-intercalated covalent organic frameworks, Adv. Energy Mater. 13 (2023) 2203695.
[6] B. He, C. Bie, X. Fei, B. Cheng, J. Yu, W. Ho, A.A. Al-Ghamdi, S. Wageh, Enhancement in the photocatalytic H_2 production activity of CdS NRs by Ag_2S and NiS dual cocatalysts, Appl. Catal. B-Environ. 288 (2021) 119994.
[7] S. Yang, H. Lv, H. Zhong, D. Yuan, X. Wang, R. Wang, Transformation of covalent organic frameworks from nacylhydrazone to oxadiazole linkages for smooth electron transfer in photocatalysis, Angew. Chem. Int. Ed. 61 (2022) e202115655.
[8] X. Kong, H. Huang, Z. Li, Y. Liang, Z. Li, S. Zhu, Facile synthesis of defected TiO_{2-x} (B) nanosheet/graphene oxide hybrids with high photocatalytic H_2 activity, J. Mater. Sci. Technol. 80 (2021) 171–178.
[9] Z. Zhao, Y. Zheng, C. Wang, S. Zhang, J. Song, Y. Li, S. Ma, P. Cheng, Z. Zhang, Y. Chen, Fabrication of robust covalent organic frameworks for enhanced visible-light-driven H_2 evolution, ACS Catal. 11 (2021) 2098–2107.
[10] H. Wang, H. Wang, Z. Wang, L. Tang, G. Zeng, P. Xu, M. Chen, T. Xiong, C. Zhou, X. Li, D. Huang, Y. Zhu, Z. Wang, J. Tang, Covalent organic framework photocatalysts: structures and applications, Chem. Soc. Rev. 49 (2020) 4135–4165.
[11] Y. Xiang, W. Dong, P. Wang, S. Wang, X. Ding, F. Ichihara, Z. Wang, Y. Wada, S. Jin, Y. Weng, H. Chen, J. Ye, Constructing electron delocalization channels in covalent organic frameworks powering CO_2 photoreduction in water, Appl. Catal. B-Environ. 274 (2020) 119096.
[12] M.R. Rao, Y. Fang, S.D. Feyter, D.F. Perepichka, Conjugated covalent organic frameworks via Michael addition-elimination, J. Am. Chem. Soc. 139 (2017) 2421–2427.
[13] L. Zou, R. Sa, H. Zhong, H. Lv, X. Wang, R. Wang, Photoelectron transfer mediated by the interfacial electron effects for boosting visible-light-driven CO_2 reduction, ACS Catal. 12 (2022) 3550–3557.
[14] L. Stegbauer, S. Zech, G. Savasci, T. Banerjee, F. Podjaski, K. Schwinghammer, C. Ochsenfeld, B.V. Lotsch, Tailor-made photoconductive pyrene-based covalent organic frameworks for visible-light driven hydrogen generation, Adv. Energy Mater. 8 (2018) 1703278.
[15] P. Pachfule, A. Acharjya, J. Roeser, T. Langenhahn, M. Schwarze, R. Schomacker, A. Thomas, J. Schmidt, Diacetylene functionalized covalent organic framework (COF) for photocatalytic hydrogen generation, J. Am. Chem. Soc. 140 (2018) 1423–1427.
[16] X. Wang, L. Chen, S.Y. Chong, M.A. Little, Y. Wu, W.H. Zhu, R. Clowes, Y. Yan, M. A. Zwijnenburg, R.S. Sprick, A.I. Cooper, Sulfone-containing covalent organic frameworks for photocatalytic hydrogen evolution from water, Nat. Chem. 10 (2018) 1180–1189.
[17] T. He, W. Zhen, Y. Chen, Y. Guo, Z. Li, N. Huang, Z. Li, R. Liu, Y. Liu, X. Lian, C. Xue, T.C. Sum, W. Chen, D. Jiang, Integrated interfacial design of covalent organic framework photocatalysts to promote hydrogen evolution from water, Nat. Commun. 14 (2023) 329.
[18] H. Dong, X.B. Meng, X. Zhang, H.L. Tang, J.W. Liu, J.H. Wang, J.Z. Wei, F. M. Zhang, L.L. Bai, X.J. Sun, Boosting visible-light hydrogen evolution of covalent-organic frameworks by introducing Ni-based noble metal-free co-catalyst, Chem. Eng. J. 379 (2020) 122342.
[19] M.Y. Gao, C.C. Li, H.L. Tang, X.J. Sun, H. Dong, F.M. Zhang, Boosting visible-light-driven hydrogen evolution of covalent organic frameworks through compositing with MoS_2: a promising candidate of noble-metal-free photocatalysts, J. Mater. Chem. A. 7 (2019) 20193–20200.
[20] S. Chandrasekaran, C. Bowen, P. Zhang, Z. Li, Q. Yuan, X. Ren, L. Deng, Spinel photocatalysts for environmental remediation, hydrogen generation, CO_2 reduction and photoelectrochemical water splitting, J. Mater. Chem. A. 6 (2018) 11078–11104.
[21] M. Chen, J. Zhao, Y. Wang, X. Huang, Y. Xu, $CuCoO_x/BiVO_4$ multifunctional catalyst for organics degradation, water oxidation, and O_2 reduction under visible light, J. Hazard. Mater. 419 (2021) 126515.
[22] M. Jiang, Y. Gao, Z. Wang, Z. Ding, Photocatalytic CO_2 reduction promoted by a $CuCo_2O_4$ cocatalyst with homogeneous and heterogeneous light harvesters, Appl. Catal. B-Environ. 198 (2016) 180–188.
[23] D. Yang, J. Feng, L. Jiang, X. Wu, L. Sheng, Y. Jiang, T. Wei, Z. Fan, Photocatalyst interface engineering: spatially confined growth of $ZnFe_2O_4$ within graphene networks as excellent visible-light-driven photocatalysts, Adv. Funct. Mater. 25 (2015) 7080–7087.
[24] Z. Wamg, H. Zhang, J. Li, Accelerated discovery of stable spinels in energy systems via machine learning, Nano Energy 81 (2021) 105665.
[25] W. Xue, W. Chang, X. Hu, J. Fan, X. Bai, E. Liu, Highly dispersed copper cobalt oxide nanoclusters decorated carbon nitride with efficient heterogeneous interfaces for enhanced H_2 evolution, J. Colloid Interface Sci. 576 (2020) 203–216.
[26] K.T. Alali, Z. Lu, H. Zhang, J. Liu, Q. Liu, R. Li, K. Aljebawi, J. Wang, P-p heterojunction $CuO/CuCo_2O_4$ nanotubes synthesized via electrospinning technology for detecting n-propanol gas at room temperature, Inorg. Chem. Front. 4 (2017) 1219–1230.
[27] J. Liu, C. Xiong, S. Jiang, X. Wu, S. Song, Efficient evolution of reactive oxygen species over the coordinated π-delocalization g-C_3N_4 with favorable charge transfer for sustainable pollutant elimination, Appl. Catal. B-Environ. 249 (2019) 282–291.
[28] X. Zhao, D. Han, M. Dai, Y. Fan, Z. Wang, D. Han, L. Niu, Direct Z-scheme FeV_2O_4/g-C_3N_4 binary catalyst for highly selective reduction of carbon dioxide, Chem. Eng. J. 436 (2022) 132051.
[29] R. Wang, W. Yu, N. Fang, P. Wang, Y. Chu, S. Wu, J. Liang, Constructing fast charge separation of $ZnIn_2S_4$@$CuCo_2S_4$ p-n heterojunction for efficient photocatalytic hydrogen energy recovery from quinolone antibiotic wastewater, Appl. Catal. B-Environ. 341 (2024) 123284.
[30] G. Lin, L. Sun, G. Huang, Q. Chen, S. Fang, J. Bi, L. Wu, Direct Z-scheme copper cobaltite/covalent triazine-based framework heterojunction for efficient photocatalytic CO_2 reduction under visible light, Sustain. Energy Fuels 5 (2021) 732–739.
[31] W. He, L. Liu, T. Ma, H. Han, J. Zhu, Y. Liu, Z. Fang, Z. Yang, K. Guo, Controllable morphology $CoFe_2O_4$/g-C_3N_4 p-n heterojunction photocatalysts with built-in electric field enhance photocatalytic performance, Appl. Catal. B-Environ. 306 (2022) 121107.
[32] X. Chen, S. Cai, E. Yu, J. Li, J. Chen, H. Jia, Photothermocatalytic performance of ACo_2O_4 type spinel with light-enhanced mobilizable active oxygen species for toluene oxidation, Appl. Surf. Sci. 484 (2019) 479–488.
[33] P. Wang, Y. Peng, C. Zhu, R. Yao, H. Song, L. Kun, W. Yang, Single-phase covalent organic framework staggered stacking nanosheet membrane for CO_2-selective separation, Angew. Chem. Int. Ed. 60 (2021) 19047–19052.
[34] A. Pendashteh, S.E. Moosavifard, M.S. Rahmanifar, Y. Wang, M.F. El-Kady, R. B. Kaner, M.F. Mousavi, Highly ordered mesoporous $CuCo_2O_4$ nanowires, a promising solution for high-performance supercapacitors, Chem. Mater. 27 (2015) 3919–3926.
[35] D. Shang, D. Li, B. Chen, B. Luo, Y. Huang, W. Shi, 2D–2D SnS2/covalent organic framework heterojunction photocatalysts for highly enhanced solar-driven hydrogen evolution without cocatalysts, ACS Sustain. Chem. Eng. 9 (2021) 14238–14248.
[36] Y. Xing, L. Yin, Y. Zhao, Z. Du, H.Q. Tan, X. Qin, W. Ho, T. Qiu, Y. Li, Construction of the 1D covalent organic framework/2D g-C_3N_4 heterojunction with high apparent quantum efficiency at 500 nm, ACS Appl. Mater. Interfaces 12 (2020) 51555–51562.

[37] Y. Shi, B. Yu, K. Zhou, R.K. Yuen, Z. Gui, Y. Hu, S. Jiang, Novel $CuCo_2O_4$/graphitic carbonnitride nanohybrids: Highly effective catalysts for reducing CO generation and fire hazardsof thermoplastic polyurethane nanocomposites, J. Hazard. Mater. 293 (2015) 87–96.
[38] K. Artyushkova, B. Kiefer, B. Halevi, A. Knop-Gericke, R. Schlogl, P. Atanassov, Density functional theory calculations of XPS binding energy shift for nitrogen-containing graphene-like structures, Chem. Commun. 49 (2013) 2539–2541.
[39] A. Ishikawa, T. Takata, J.N. Kondo, M. Hara, H. Kobayashi, K. Domen, Oxysulfide $Sm_2Ti_2S_2O_5$ as a stable photocatalyst for water oxidation and reduction under visible light irradiation ($\lambda \leq 650$ nm), J. Am. Chem. Soc. 124 (2002) 13547–13553.
[40] Z. Wang, P.K. Nayak, J.A. Caraveo-Frescas, H.N. Alshareef, Recent developments in p-type oxide semiconductor materials and devices, Adv. Mater. 28 (2016) 3831–3892.
[41] H. Lv, P. Li, X. Li, X. Li, A. Chen, R. Sa, H. Zhu, R. Wang, Boosting photocatalytic reduction of the diluted CO_2 over covalent organic framework, Chem. Eng. J. 451 (2023) 138745.
[42] Y. Wang, P. Dong, K. Zhu, A. Zhang, J. Pan, Z. Chen, Z. Li, R. Guan, X. Xi, J. Zhang, Embedding $[Mo_3S_{13}]^{2-}$ clusters into the micropores of a covalent organic framework for enhanced stability and photocatalytic hydrogen evolution, Chem. Eng. J. 446 (2022) 136883.
[43] Y. Xu, X. He, H. Zhong, D. Singh, L. Zhang, R. Wang, Solid salt confinement effect: an effective strategy to fabricate high crystalline polymer carbon nitride for enhanced photocatalytic hydrogen evolution, Appl. Catal. B-Environ. 246 (2019) 349–355.